Experimental Evidence for the Existence of the Ultimate Regime in Rapidly Rotating Turbulent Thermal Convection

Hechuan Jiang,[1,2,*] Dongpu Wang,[1,*] Shuang Liu,[1,3] and Chao Sun[1,4,†]
[1]Center for Combustion Energy, Key Laboratory for Thermal Science and Power Engineering of MoE, and Department of Energy and Power Engineering, Tsinghua University, 100084 Beijing, China
[2]Huaneng Clean Energy Research Institute, 102209 Beijing, People's Republic of China
[3]Yau Mathematical Sciences Center, Tsinghua University, 100084 Beijing, China
[4]Department of Engineering Mechanics, School of Aerospace Engineering, Tsinghua University, 100084 Beijing, China

(Received 10 January 2022; accepted 20 October 2022; published 10 November 2022)

What is the final state of turbulence when the driving parameter approaches infinity? For the traditional Rayleigh-Bénard convection, a possible ultimate scaling dependence of the heat transport (quantified by the Nusselt number Nu) on the Rayleigh number (Ra), which can be extrapolated to arbitrarily high Ra, is predicted by theories. The existence of the ultimate scaling has been intensively debated in the past decades. In this Letter, we adopt a novel supergravitational thermal convection experimental setup to study the possible transition to the ultimate regime. This system is characterized by the combined effects of radial-dependent centrifugal force, the Earth's gravity, and the Coriolis force. With an effective gravity up to 100 times the Earth's gravity, both Ra and shear Reynolds number can be boosted due to the increase of the buoyancy driving and the additional Coriolis forces. With over a decade of Ra range, we demonstrate the existence of ultimate regime with four direct evidences: the ultimate scaling dependence of Nu versus Ra; the appearance of the turbulent velocity boundary layer profile; the enhanced strength of the shear Reynolds number; and the new statistical properties of local temperature fluctuations. The present findings will greatly improve the understanding of the flow dynamics in geophysical and astrophysical flows.

DOI: 10.1103/PhysRevLett.129.204502

Thermally driven turbulent flows ubiquitously occur in meteorological [1], geophysical [2,3], and astrophysical [4,5] flows and industrial processes [6]. A paradigm for modeling the thermally driven turbulent flows is Rayleigh-Bénard convection (RBC) (see Refs. [7–9] for reviews), which is a layer of fluid confined between two horizontal plates heated from below and cooled from above. The direction of gravity is the same as the temperature gradient. In those aforementioned natural phenomena, the driving strength of the flow is extremely high and far beyond the accessible regime in the lab scales. A powerful approach for the investigation of these natural phenomena and industrial processes using laboratory experiments is to find the asymptotic laws that can extrapolate the laboratory findings to the unattainable parameter regimes in the natural and industrial systems. One example of such asymptotic laws is the dependence of the Nusselt number Nu (dimensionless convective heat flux) on the Rayleigh number Ra (dimensionless strength of driving buoyancy) in the limit of intense thermal forcing. In 1962, Kraichnan's seminal work predicted as Ra increases, thermal convection will reach an ultimate regime with $\mathrm{Nu} \propto \mathrm{Ra}^{1/2}(\ln \mathrm{Ra})^{-3/2} \propto \mathrm{Ra}^{\gamma}$ [10], which yields a steeper effective scaling exponent ($\gamma > 1/3$, and asymptotically approaches to $1/2$) as compared to the scaling exponent ($\gamma \lesssim 1/3$) in the classical regime before the transition, where the turbulent transport is limited by laminar boundary layers (BLs).

In the past 40 years, a large number of studies attempted to search for this ultimate scaling in high Ra regimes [11–21]. For the reported experimental results, most Nu(Ra) measurements are consistent below $\mathrm{Ra} \simeq 10^{11}$–$10^{12}$, while the situation at larger Ra becomes puzzling. At $\mathrm{Ra} \gtrsim 10^{11}$, the compensated heat transport $\mathrm{Nu}\,\mathrm{Ra}^{-1/3}$ decreases or levels out with Ra in some studies [11,13,14,17,19,22] while it increases in others [12,15,16,18,20,21]. For numerical simulations, limited by the power of supercomputers, three-dimensional direct numerical simulations (DNS) can only reach $\mathrm{Ra} = 2 \times 10^{12}$ for a moderate aspect ratio between the diameter and height of the convection cell [23], which does not show the transition to the ultimate regime. For both experiments and simulations, it is notoriously difficult to arrive at very high Ra while keeping other parameters as constants. Recently, signatures of the transition to ultimate regime have been reported in the experimental studies of traditional RBC [16].

In this Letter, we explore the ultimate regime of thermal turbulence in a supergravitational thermal convection system through rapid rotation. We adopt a supergravitational system (Annular Centrifugal RBC, ACRBC) [sketched in Fig. 1(a)], which is a cylindrical annulus with cooled inner and heated outer walls under a rapid solid-body rotation [24–27]. The direction of centrifugal force (effective gravity) is the same as the temperature gradient,

which is consistent with classical RBC. The details about the experiments and DNS can be found in the Supplemental Material, Secs. I–III [28]. A similar system has been used to study baroclinic waves, zonal flow, and convection in the low Ra regime [29–33,51–56]. Here, we exploit the rapidly rotating system to study high Ra thermal turbulence.

The flow dynamics in ACRBC are determined by the following control parameters, namely the Rayleigh number

$$\mathrm{Ra} = \frac{1}{2}\omega^2(R_o + R_i)\beta\Delta L^3/(\nu\kappa), \tag{1}$$

the inverse Rossby number

$$\mathrm{Ro}^{-1} = 2[\beta\Delta(R_o + R_i)/(2L)]^{-1/2}, \tag{2}$$

the Prandtl number $\mathrm{Pr} = \nu/\kappa$, and radius and aspect ratios $\eta = R_i/R_o$, $\Gamma_\perp = H/L$, and $\Gamma_\parallel = 2\pi r/L$. Here β, Δ, ν, and κ are the thermal expansion coefficient, the temperature difference between hot and cold walls, the kinematic viscosity, and the thermal diffusivity of the working fluid, respectively. The angular velocity ω is canceled out and does not appear in the definition of Ro^{-1}. The key response parameter is Nusselt number $\mathrm{Nu} = J/J_{\mathrm{con}} = -JR_o \ln\eta/(\alpha\Delta)$, where J, J_{con}, and α denote the total heat flux, the heat flux through pure thermal conduction, and thermal conductivity, respectively.

According to the definition of Ra, we can push Ra to higher values through increasing ω of the system and increasing $\beta/(\nu\kappa)$ of the working fluid. The range of rotation rate is from 211 rpm to 705 rpm, corresponding to an effective gravity [8.9 g, 100 g]. The Earth's gravity does not play an important role in the current parameter regime (see Ref. [24] for detailed discussion). Next to the degassed water at around 40 °C, we use Novec 7200 (3M Inc. Engineered Fluid) at around 25 °C as the working fluid, which has roughly 14.4 times of $\beta/(\nu\kappa)$ as compared with water. The properties of the Novec 7200 are listed in the Supplemental Material, Sec. III [28].

The explored parameter space is shown in Figs. 1(b) and 1(c). We have performed 62 experiments and 44 numerical simulations in total. The details about the experimental and numerical cases are documented in the Supplemental Material, Sec. XI [28]. Combining experiments and simulations, the range of Ra explored here extends almost six and a half decades, i.e., from 10^6 to 3.7×10^{12}. In experiments, the Earth's gravity, lids, and inhomogeneity of centrifugal force have been studied in Ref. [24], which shows that their effects on Nu are negligible. In addition, the non-Oberbeck-Boussinesq (NOB) effects [57] are negligible for all of our data, and we discuss the NOB effects in the Supplemental Material, Sec. X [28].

Figure 2(a) shows the obtained Nu as a function of Ra from experiments and numerical simulations. For most experiments, the measurement lasts at least 4 hours after the system has reached a statistically stationary state (for the detailed measurements, see the Supplemental Material, Sec. III) [28]. Since two kinds of working fluids are used in the experiments, the difference in Pr should be taken into account. A previous study suggested that Nu has a weak dependence on Pr in this Pr range [4, 10.7] and the scaling law can be written as $\mathrm{Nu} \sim \mathrm{Pr}^{-0.03}$ [50,58,59]; therefore, all Nu data, including the data at $\mathrm{Pr} \approx 10.4$ (Novec 7200) and the data at $\mathrm{Pr} \approx 4.3$ (water), have been corrected with $\mathrm{Nu}/(\mathrm{Pr}/4.3)^{-0.03}$ to coincide with the data for water at 40 °C. It is evident that the experiments for Novec 7200 and water and numerical simulations are all in an excellent agreement. In the range of Ro^{-1} from 9 to 58, the datasets show a consistent dependence of Nu on Ra. To better demonstrate the local scaling exponent, Fig. 2(b) shows the same plot as Fig. 2(a) but in a compensated way. In ACRBC, an effective scaling of $\mathrm{Nu} \propto \mathrm{Ra}^{0.27}$ is observed when $\mathrm{Ra} < 10^{10}$, and the scaling exponent is close to the value found in two-dimensional (2D) RBC [44,60] where the viscous BLs are laminar. Note, in ACRBC, the flow has a quasi-2D structure at the current Ro range ($\mathrm{Ro}^{-1} \geqslant 9$) for Nu measurements [24]. The findings of classical regime in ACRBC give independent support for the previous results on RBC [15,61] and Taylor-Couette turbulence [62,63].

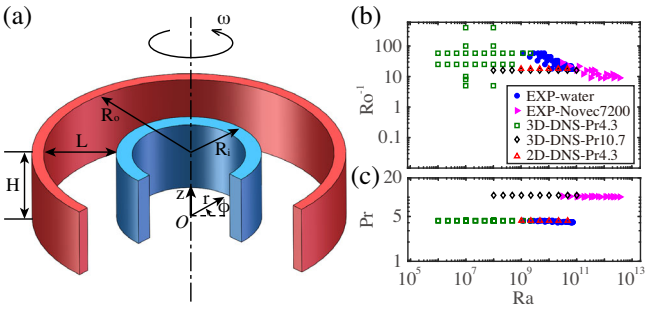

FIG. 1. Experimental configuration and explored parameter space. (a) Schematical diagram of the system, which defines the coordinate frame and geometric parameters. (b) Phase diagrams of Ro^{-1} and Ra, where solid symbols and open symbols denote the experimental data and DNS data, respectively. (c) Phase diagrams but in the Pr-Ra plane.

Once the Ra increases beyond 10^{10}, the system enters a transition regime with local effective scaling exponent γ of $\mathrm{Nu} \propto \mathrm{Ra}^{\gamma}$ increasing from $\gamma = 0.27$ to $\gamma > 1/3$ as evident from the arc bottom in the compensated plot. Surprisingly, following the transition regime, there is a steep scaling regime with a local scaling exponent $\gamma = 0.40 \pm 0.01$, which spans more than one decade from $\mathrm{Ra} \sim 10^{11}$ to $\mathrm{Ra} = 3.7 \times 10^{12}$. This steep scaling exponent is consistent with the prediction for Nu(Ra) of the Grossmann-Lohse theory in the ultimate regime with logarithmic corrections [66]. We also perform a direct fitting in the range of $10^{11} \leq \mathrm{Ra} \leq 4 \times 10^{12}$ according to the Kraichnan's theory $\mathrm{Nu} \sim \mathrm{Ra}^{1/2}(\ln \mathrm{Ra})^{-3/2}$, and the fitting result is acceptable basically (see Fig. 15 of the

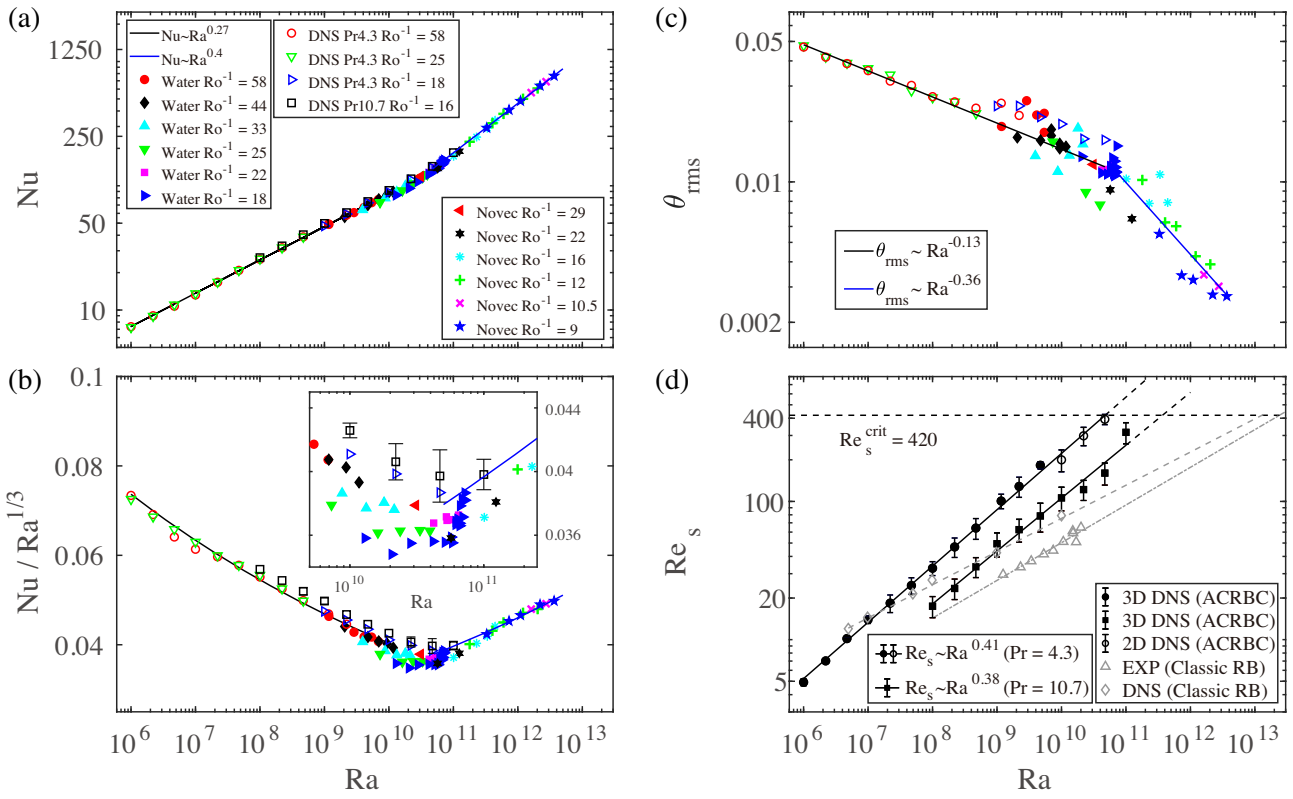

FIG. 2. Global heat transport, temperature fluctuation, and shear Reynolds number. (a) Nusselt number Nu as a function of Rayleigh number Ra; (b) the compensated plots of $\mathrm{Nu}/\mathrm{Ra}^{1/3}$ versus Ra; (c) the normalized rms of temperature fluctuation θ_{rms} in the bulk region versus Ra; (d) the shear Reynolds number Re_s as a function of Ra. In panel (a), the solid lines are the best fitting of the experimental and DNS data in ACRBC at two different regimes. To eliminate the weak influence of Pr difference, Nusselt numbers are corrected with $\mathrm{Nu}/(\mathrm{Pr}/4.3)^{-0.03}$ [50,58,59]. In panel (b), the inset shows the enlarged part near the transition Ra. In panel (d), the extrapolations of the fitting of DNS results for water ($\mathrm{Ro}^{-1} = 18$ and 58) and Novec ($\mathrm{Ro}^{-1} = 16$) indicate that the BL becomes turbulent ($\mathrm{Re}_s = 420$, dashed line) at $\mathrm{Ra} \simeq 10^{11}$. Shear Reynolds numbers from experiments [64] and from DNS [65] in classical RBC system are also plotted for comparison.

Supplemental Material, Sec. V [28]). Here, we should note that the maximum Ra ($\mathrm{Ra} = 10^{11}$) for the present simulation is not sufficient to study the ultimate regime. (The limits of the simulation are discussed in the Supplemental Material, Secs. VII [28] and XI [28]).

What is the reason for the enhanced Nu scaling? Could this be due to the transition of the flow structure from a two-dimensional flow state to a three-dimensional state, which results in a locally higher Nu? The minimum $\mathrm{Ro}^{-1} = 9$ corresponds to the temperature difference $\Delta = 20$ K, which suggests Coriolis force still dominates the flow dynamics. In addition, the flow transition from two-dimensional to three-dimensional is not likely to occur as this process is complicated [24], while a scaling law ($\mathrm{Nu} \sim \mathrm{Ra}^{0.4}$) is found for different Ro^{-1} and $\mathrm{Ra} \in [10^{11}, 3.7 \times 10^{12}]$. So the enhancement of local scaling exponent is probably not attributed to the change of flow state from two-dimensional to three-dimensional. We note that there exist four pairs of rolls in ACRBC both in the classical (Fig. 17 in the Supplemental Material) and ultimate (Fig. 16 in the Supplemental Material) regime, indicating that the transition does not result from the change of large-scale 2D pattern [67,68]. Thus we consider the physical reason might be that the transition Ra to the ultimate regime in ACRBC is lower than that in the traditional RBC (to be discussed below).

He *et al.* [69–71] found that the wall-normal profiles of the temperature variance in the ultimate regime (logarithmic profile) are different from that in the classical regime (power-law profile). Here, we explore the normalized root-mean-square temperature fluctuation θ_{rms} in the bulk region as a function of Ra [Fig. 2(c)]. It is evident that there is a transition in the variation trend of θ_{rms} vs. Ra at exactly the critical Rayleigh number $\mathrm{Ra}_t \simeq 10^{11}$ where the Nu scaling changes. The obtained scaling $\theta_{\mathrm{rms}} \sim \mathrm{Ra}^{-0.13\pm0.02}$ for $\mathrm{Ra} < \mathrm{Ra}_t$ is consistent with previous studies for the classical RBC [11,13,72], while it gives a notably steeper scaling with $\theta_{\mathrm{rms}} \sim \mathrm{Ra}^{-0.36\pm0.05}$ when $\mathrm{Ra} > \mathrm{Ra}_t$. The bulk temperature fluctuation is suggested to be dominated by contributions of detached plumes from the BLs [11]. This change of the scaling exponent of θ_{rms} versus Ra in the ultimate regime indicates the significant change in the properties of the BL where the plumes are emitted.

The next key question is why is the transition Rayleigh number ($\mathrm{Ra}_t \sim 10^{11}$) 3 orders of magnitude lower than that in the traditional RBC system [16] ($\mathrm{Ra}_t \sim 10^{14}$)?

The key ingredient of the transition from classical regime to ultimate regime is the change of BL properties, i.e., the transition from laminar BL to a turbulent one [10,66,73]. The properties of BL critically depend on the shear Reynolds number. A typical value for the onset of turbulence is $\mathrm{Re}_s^{\mathrm{crit}} \approx 420$ [74]. We now analyze Re_s as a function of Ra in the current system and compare it to that in the classical RBC system. It is difficult to directly measure the shear Reynolds number from the experiments due to the rapid rotation and very small scale of the BL. Fortunately, we can evaluate Re_s using the DNS data. Figure 2(d) shows the calculated shear Reynolds number, $\mathrm{Re}_s = U\lambda_u/\nu$, based on the DNS results; here U is the maximum of temporally and spatially averaged azimuthal velocity, and λ_u is the viscous BL thickness estimated with the commonly used "slope method" [75]. As shown in Fig. 2(d), the shear Reynolds number monotonously increases with Ra with an effective scaling around $\mathrm{Re}_s \sim \mathrm{Ra}^{0.41\pm0.01}$ for $Pr = 4.3$ and $\mathrm{Re}_s \sim \mathrm{Ra}^{0.38\pm0.01}$ for $\mathrm{Pr} = 10.7$. These scaling exponents are much larger in the current system than that in the classical RBC. The magnitude of Re_s is also much larger than that in the classical RBC. It already arrives at the critical shear Reynolds number of 420 [74] at $\mathrm{Ra} \simeq 10^{11}$, whereas the shear Reynolds number at the same Ra in the classical system is around 80 [64,65].

To understand the steep scaling of the shear Reynolds number in rapidly rotating ACRBC, we derive the theoretical scalings according to the dominated forces in both the traditional RBC and ACRBC. Regarding the scaling of Re_s with Ra, we consider the force balance of the BL flow based on the momentum transport equation in the large-scale circulation plane. For traditional RBC, the balance of the inertial term $\vec{u}\cdot\nabla\vec{u}$ and the viscous term $\nu\nabla^2\vec{u}$ gives the classical scaling of the viscous BL, $\lambda_u/L \sim \mathrm{Re}^{-1/2}$ and $\mathrm{Re}_s \sim \mathrm{Re}^{1/2}$. Whereas in ACRBC, when rotation is rapid enough such that the Coriolis force $2\vec{\omega}\times\vec{u}$ plays an important role in the BL flow, one would expect a balance between the Coriolis force and the viscous force, which results in a new scaling behavior, $\lambda_u/L \sim \mathrm{Re}^{-1/3}$ and $\mathrm{Re}_s \sim \mathrm{Re}^{2/3}$. Together with the effective scaling law $\mathrm{Re} \sim \mathrm{Ra}^{0.55}$, the new scaling gives rise to the scaling law $\mathrm{Re}_s \sim \mathrm{Ra}^{0.37}$, close to the observation in Fig. 2(d). The detailed derivation of $\mathrm{Re}_s \sim \mathrm{Ra}$ scaling can be referred to the Supplemental Material, Sec. VIII [28]. Thus, the dominance of Coriolis force yields the steep scaling of Re_s with Ra and thus results in the early transition of ACRBC to the ultimate regime at $\mathrm{Ra}_t \sim 10^{11}$.

Figure 3 shows the temporally and spatially averaged azimuthal velocity profiles in wall units for different Ra from DNS. In wall units, the mean azimuthal velocity $|u|^+$ is normalized by the friction velocity $u_\tau = \sqrt{\nu\partial_r\langle u\rangle|_{R_i,R_o}}$,

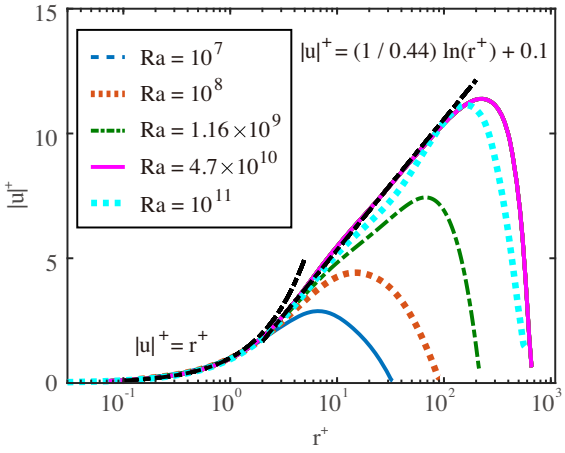

FIG. 3. Mean boundary layer velocity profiles in wall units at different Ra, $\mathrm{Ra} = 10^7$–4.7×10^{10} ($\mathrm{Ro}^{-1} = 18, 58$ and $\mathrm{Pr} = 4.3$) and $\mathrm{Ra} = 10^{11}$ ($\mathrm{Ro}^{-1} = 16$ and $\mathrm{Pr} = 10.7$), u^+ for velocity, and r^+ for wall distance. The black dash-dotted lines show the viscous sublayer behavior $|u|^+ = r^+$ and log-layer behavior $|u|^+ = (1/\kappa)\ln(r^+) + B$ with $\kappa = 0.44$ and $B = 0.10$.

and radial position r^+ is normalized by the viscous length scale $\delta_\nu = \nu/u_\tau$ [76]. The profiles of viscous sublayer ($|u|^+ = r^+$) and Prandtl-von Kármán type BL [$|u|^+ = (1/\kappa)\ln(r^+) + B$] [77] are also plotted for comparison. We show that when Ra is small, the profile behaves as the laminar Prandtl-Blasius type. With Ra increasing, the BL profile progressively approaches towards a Prandtl-von Kármán (logarithmic) type. At $\mathrm{Ra} = 4.7\times10^{10}$ and 10^{11}, a logarithmic range is notable over one decade of r^+, which is an essential indication of the emergence of turbulent BL. The inverse slope $\kappa = 0.44$ of the obtained logarithmic law is quite close to the typical von Kármán constant $\kappa = 0.41$ despite the different flow configurations. The parameter $B = 0.10$ is different from the classical Prandtl-von Kármán value for canonical turbulent BLs over smooth walls, which may be attributed to the finite values of Ra reached in the DNS and the complicated interactions between velocity shear, unstable thermal stratification, the Coriolis force, and curvature effect in ACRBC. Nevertheless, the fact that the velocity profile shows the typical characteristics of a turbulent BL illustrates the onset of turbulence in the BL flow. Unfortunately, higher Ra simulation has not been achieved in the present study. The above analysis gives an indication that the strong shear and Coriolis effects induced by rapid rotation promote the BL transition to the turbulent Prandtl-von Kármán type [25].

In summary, by means of dramatically increased driving force and strong shear induced by rapid rotation, the transition to the ultimate regime of thermal convection is observed in an annular centrifugal Rayleigh-Bénard convection system. We have performed extensive experiments and numerical simulations to study the heat transport and flow dynamics in ACRBC from classical regime to ultimate regime. For $\mathrm{Ra} \lesssim 10^{10}$, $\mathrm{Nu}(\mathrm{Ra})$ is consistent with classical

RBC as expected. For $\mathrm{Ra} \gtrsim 10^{11}$, the measured local effective Nu scaling exponent γ increases to 0.40, spanning more than one decade of Ra range, which testifies to the possible transition to ultimate regime. As a response to the transition to ultimate regime, the dependence of temperature fluctuations on Ra demonstrates different scaling behaviors before Ra_t and beyond Ra_t. The steep Ra dependence of the shear Reynolds number leads to a smaller transition Rayleigh number Ra_t at which the shear Reynolds number crosses $\mathrm{Re}_s = 420$. Approaching the transition Ra_t, the mean velocity profile has a log layer spanning over one decade of r^+ in wall units. In view of these above evidences, it could be concluded that transition to the ultimate state of thermal convection has been realized for the supergravitational thermal convection system. While our data suggest that the transition to the ultimate state is determined by the critical shear Reynolds number of the velocity BL, some recent studies found Ra_t is also affected by the Prandtl number [22] and aspect ratio [78,79] in traditional RBC. Some unique effects in ACRBC like curvature effect, the Coriolis force, the radial-dependent supergravity, and the Earth's gravity may also change the onset of the transition. Hence, more studies are needed to further verify this transition to ultimate regime of thermal turbulence.

We thank Guenter Ahlers, Eberhard Bodenschatz, Detlef Lohse, Roberto Verzicco, Ke-Qing Xia, Yantao Yang, Quan Zhou, and Xiaojue Zhu for insightful discussions over the years, and thank Gert-Wim Bruggert and Sander Huisman for the technical assistance with the setup. This work is financially supported by the National Natural Science Foundation of China under Grants No. 11988102 and No. 91852202, and Tencent Foundation through the XPLORER PRIZE.

*These authors are equally contributed to this work.
†chaosun@tsinghua.edu.cn

[1] J. C. Wyngaard, Annu. Rev. Fluid Mech. **24**, 205 (1992).
[2] W. M. Telford, Nature (London) **216**, 143 (1967).
[3] M. Yoshida, Phys. Fluids **30**, 096601 (2018).
[4] J. Schumacher and K. R. Sreenivasan, Rev. Mod. Phys. **92**, 041001 (2020).
[5] S. M. Hanasoge, H. Hotta, and K. R. Sreenivasan, Sci. Adv. **6**, eaba9639 (2020).
[6] J. M. Owen and C. A. Long, Journal of turbomachinery **137**, 11 (2015).
[7] G. Ahlers, S. Grossmann, and D. Lohse, Rev. Mod. Phys. **81**, 503 (2009).
[8] D. Lohse and K. Q. Xia, Annu. Rev. Fluid Mech. **42**, 335 (2010).
[9] F. Chillà and J. Schumacher, Eur. Phys. J. E **35**, 58 (2012).
[10] R. H. Kraichnan, Phys. Fluids **5**, 1374 (1962).
[11] B. Castaing, G. Gunaratne, F. Heslot, L. Kadanoff, A. Libchaber, S. Thomae, X. Z. Wu, S. Zaleski, and G. Zanetti, J. Fluid Mech. **204**, 1 (1989).
[12] X. Chavanne, F. Chillà, B. Castaing, B. Hébral, B. Chabaud, and J. Chaussy, Phys. Rev. Lett. **79**, 3648 (1997).
[13] J. Niemela, L. Skrbek, K. R. Sreenivasan, and R. J. Donnelly, Nature (London) **404**, 837 (2000).
[14] J. J. Niemela, S. Babuin, and K. R. Sreenivasan, J. Fluid Mech. **649**, 509 (2010).
[15] P. E. Roche, F. Gauthier, R. Kaiser, and J. Salort, New J. Phys. **12**, 085014 (2010).
[16] X. He, D. Funfschilling, H. Nobach, E. Bodenschatz, and G. Ahlers, Phys. Rev. Lett. **108**, 024502 (2012).
[17] P. Urban, P. Hanzelka, V. Musilová, T. Králík, M. L. Mantia, A. Srnka, and L. Skrbek, New J. Phys. **16**, 053042 (2014).
[18] G. Ahlers, E. Bodenschatz, and X. He, Phys. Rev. Fluids **2**, 054603 (2017).
[19] K. P. Iyer, J. D. Scheel, J. Schumacher, and K. R. Sreenivasan, Proc. Natl. Acad. Sci. U.S.A. **117**, 7594 (2020).
[20] X. He, E. Bodenschatz, and G. Ahlers, Proc. Natl. Acad. Sci. U.S.A. **117**, 30022 (2020).
[21] K. Kawano, S. Motoki, M. Shimizu, and G. Kawahara, J. Fluid Mech. **914**, A13 (2021).
[22] L. Méthivier, R. Braun, F. Chillà, and J. Salort, Europhys. Lett. **136**, 10003 (2021).
[23] R. J. A. M. Stevens, D. Lohse, and R. Verzicco, J. Fluid Mech. **688**, 31 (2011).
[24] H. Jiang, X. Zhu, D. Wang, S. G. Huisman, and C. Sun, Sci. Adv. **6**, eabb8676 (2020).
[25] A. Rouhi, D. Lohse, I. Marusic, C. Sun, and D. Chung, J. Fluid Mech. **910**, A32 (2021).
[26] D. Wang, H. Jiang, S. Liu, X. Zhu, and C. Sun, J. Fluid Mech. **930**, A19 (2022).
[27] D. Wang, S. Liu, Q. Zhou, and C. Sun, Phys. Fluids **34**, 055108 (2022).
[28] See Supplemental Material at http://link.aps.org/supplemental/10.1103/PhysRevLett.129.204502 for Secs. I–III, which provide details about the experiments and DNS and include Refs. [7,24,25,29–43]; Sec. III, which provides details about the properties of the Novec 7200, experimental procedures, and temperature measurements and includes Refs. [25,40–43]; Sec. V, which provides details about the direct fitting using the Kraichnan's theory and includes Ref. [10]; Sec. VII, which provides details about the limits of the DNS and includes Ref. [44]; Sec. VIII, which provides details about the derivation of $\mathrm{Re}_s \sim \mathrm{Ra}$ and includes Refs. [45–47]; Sec. X, which provides details about the discussion of NOB effects and includes Refs. [34,48,49]; and Sec. XI, which provides details about the experimental and numerical cases and includes Refs. [23,50].
[29] F. Busse and C. Carrigan, J. Fluid Mech. **62**, 579 (1974).
[30] M. Azouni, E. Bolton, and F. Busse, Geophys. Astrophys. Fluid Dyn. **34**, 301 (1985).
[31] F. Busse, J. Fluid Mech. **173**, 545 (1986).
[32] F. Busse and A. Or, J. Fluid Mech. **166**, 173 (1986).
[33] F. Busse, Chaos **4**, 123 (1994).
[34] G. Ahlers, E. Brown, F. F. Araujo, D. Funfschilling, S. Grossmann, and D. Lohse, J. Fluid Mech. **569**, 409 (2006).
[35] J. M. Lopez, F. Marques, and M. Avila, J. Fluid Mech. **737**, 56 (2013).
[36] R. Verzicco and P. Orlandi, J. Comput. Phys. **123**, 402 (1996).

[37] E. P. van der Poel, R. Ostilla-Mónico, J. Donners, and R. Verzicco, Comput. Fluids **116**, 10 (2015).
[38] X. Zhu *et al.*, Comput. Phys. Commun. **229**, 199 (2018).
[39] X. Zhu, R. A. Verschoof, D. Bakhuis, S. G. Huisman, R. Verzicco, C. Sun, and D. Lohse, Nat. Phys. **14**, 417 (2018).
[40] J. Steinhart and S. Hart, Deep Sea Res. Oceanogr. Abstr. **15**, 497 (1968).
[41] C. Sun and Q. Zhou, Nonlinearity **27**, R89 (2014).
[42] C. Popiel and J. Wojtkowiak, Heat transfer engineering **19**, 87 (1998).
[43] E. Batista and R. Paton, Metrologia **55**, 731 (2018).
[44] E. P. van der Poel, R. J. A. M. Stevens, and D. Lohse, J. Fluid Mech. **736**, 177 (2013).
[45] K. Sugiyama, E. Calzavarini, S. Grossmann, and D. Lohse, J. Fluid Mech. **637**, 105 (2009).
[46] Y. Zhang, Q. Zhou, and C. Sun, J. Fluid Mech. **814**, 165 (2017).
[47] S. Cioni, S. Ciliberto, and J. Sommeria, J. Fluid Mech. **335**, 111 (1997).
[48] K. Sugiyama, E. Calzavarini, S. Grossmann, and D. Lohse, Europhys. Lett. **80**, 34002 (2007).
[49] J. J. Niemela and K. R. Sreenivasan, J. Fluid Mech. **481**, 355 (2003).
[50] K. Q. Xia, S. Lam, and S. Q. Zhou, Phys. Rev. Lett. **88**, 064501 (2002).
[51] W. Fowlis and R. Hide, J. At. Sci. **22**, 541 (1965).
[52] R. Hide and P. J. Mason, Adv. Phys. **24**, 47 (1975).
[53] P. Read, X. Morice-Atkinson, E. Allen, and A. Castrejón-Pita, Chaos **27**, 127001 (2017).
[54] C. Kang, A. Meyer, I. Mutabazi, and H. N. Yoshikawa, Phys. Rev. Fluids **2**, 053901 (2017).
[55] C. Kang, A. Meyer, H. N. Yoshikawa, and I. Mutabazi, Phys. Rev. Fluids **4**, 043501 (2019).
[56] R. Menaut, Y. Corre, L. Huguet, T. Le Reun, T. Alboussière, M. Bergman, R. Deguen, S. Labrosse, and M. Moulin, Phys. Rev. Fluids **4**, 033502 (2019).
[57] A. Oberbeck, Ann. Phys. Chem. **7**, 271 (1879).
[58] G. Ahlers and X. Xu, Phys. Rev. Lett. **86**, 3320 (2001).
[59] S. Grossmann and D. Lohse, Phys. Rev. Lett. **86**, 3316 (2001).
[60] X. Zhu, V. Mathai, R. J. A. M. Stevens, R. Verzicco, and D. Lohse, Phys. Rev. Lett. **120**, 144502 (2018).
[61] P. Urban, V. Musilová, and L. Skrbek, Phys. Rev. Lett. **107**, 014302 (2011).
[62] R. Ostilla-Mónico, E. P. van der Poel, R. Verzicco, S. Grossmann, and D. Lohse, J. Fluid Mech. **761**, 1 (2014).
[63] A. Froitzheim, S. Merbold, R. Ostilla-Mónico, and C. Egbers, Phys. Rev. Fluids **4**, 084605 (2019).
[64] C. Sun, Y. H. Cheung, and K. Q. Xia, J. Fluid Mech. **605**, 79 (2008).
[65] J. D. Scheel and J. Schumacher, J. Fluid Mech. **758**, 344 (2014).
[66] S. Grossmann and D. Lohse, Phys. Fluids **23**, 045108 (2011).
[67] Q. Wang, K. L. Chong, R. J. A. M. Stevens, R. Verzicco, and D. Lohse, J. Fluid Mech. **905**, A21 (2020).
[68] Q. Wang, R. Verzicco, D. Lohse, and O. Shishkina, Phys. Rev. Lett. **125**, 074501 (2020).
[69] X. He, D. P. M. van Gils, E. Bodenschatz, and G. Ahlers, Phys. Rev. Lett. **112**, 174501 (2014).
[70] X. He, E. Bodenschatz, and G. Ahlers, J. Fluid Mech. **791**, R3 (2016).
[71] X. He, E. Bodenschatz, and G. Ahlers, Theor. Appl. Mech. Lett. **11**, 100237 (2021).
[72] Y. H. Yang, X. Zhu, B. F. Wang, Y. L. Liu, and Q. Zhou, Phys. Fluids **32**, 015101 (2020).
[73] S. Grossmann and D. Lohse, J. Fluid Mech. **407**, 27 (2000).
[74] L. D. Landau and E. M. Lifshitz, *Fluid Mechanics*, 2nd ed. (Pergamon, New York, 1987), pp. 95–156.
[75] Q. Zhou and K. Q. Xia, Phys. Rev. Lett. **104**, 104301 (2010).
[76] S. Pope, *Turbulent Flows* (Cambridge University Press, Cambridge, England, 2000), pp. 269–271.
[77] A. M. Yaglom, Annu. Rev. Fluid Mech. **11**, 505 (1979).
[78] O. Shishkina, Phys. Rev. Fluids **6**, 090502 (2021).
[79] X. He, E. Bodenschatz, and G. Ahlers, J. Fluid Mech. **931**, A7 (2022).